THE JOURNAL OF PHYSICAL CHEMISTRY B

Article

pubs.acs.org/JPCB

Recombination, Dissociation, and Transport of Ion Pairs across the Liquid/Liquid Interface. Implications for Phase Transfer Catalysis

Ilan Benjamin

Department of Chemistry and Biochemistry, University of California—Santa Cruz, Santa Cruz, California 95064, United States

ABSTRACT: Molecular dynamics simulations are used to calculate several free energy profiles relevant to the recombination/dissociation and transport of individual ions and ion pairs across the water/chloroform interface. Tetra methyl ammonium (TMA^+) and tetra butyl ammonium (TBA^+) (typically used as phase transfer catalysts) and a chloride ion (as an example of a transferred nucleophile) are considered. The free-energy profiles for the transfer of the three ions and the two ion pairs (TMA^+Cl^- and TBA^+Cl^-) across the interface, as well as the potential of mean force for the dissociation of these two ion pairs at different interface locations, are calculated and correlated with structural and energetic changes at the interface. These equilibrium calculations, together with nonequilibrium trajectory calculations, provide molecular insight into the mechanism of phase transfer catalysis. In particular, water surface fluctuations are strongly coupled to the ion-pair location along the interface normal and the ion-pair bond length.

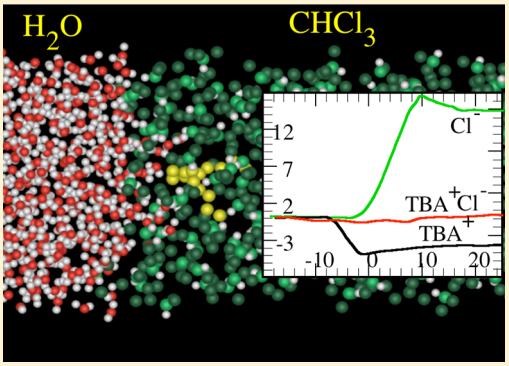

I. INTRODUCTION

Liquid–liquid phase transfer catalysis (LLPTC) is a common approach to organic synthesis involving the transfer of a water-soluble ionic reactant X^- from an aqueous phase into an organic phase, where it reacts with a water-insoluble reactant.[1−5] Once complete, the catalyst (a quaternary ammonium cation is a common example) transfers the ionic product to the aqueous phase, and the catalytic cycle repeats. This method is widely used in organic synthesis,[6] in pharmaceutical and agrochemical industries,[1] in material science,[7] and in "green" chemistry applications.[5] A schematic representation involving an S_N2 reaction is depicted in Figure 1.

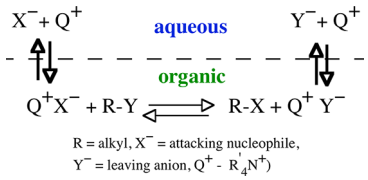

Figure 1. Schematic representation of the equilibrium and transport processes involved in liquid/liquid phase transfer catalysis.

Recently, we considered several fundamental molecular-level aspects of the LLPTC process by studying in detail the simple benchmark symmetric $Cl^- + CH_3Cl \rightarrow CH_3Cl + Cl^-$ at the water/chloroform liquid–liquid interface. By utilizing a simple two-state empirical valence bond (EVB) model, we examine the thermodynamics and dynamics of this reaction as a function of location and orientation at the interface (and the bulk), with and without the presence of a tetra methyl ammonium cation (TMA^+).[8−11] The main results of these studies were that the activation free energy of the above reaction at the interface is *equal or slightly larger* than the value in bulk water. However, the activation barrier is sensitive to the reagents' location and orientation relative to the interfacial normal, approaching the value in bulk chloroform when the reactants are located a few nm from the Gibbs dividing surface (an average interface location where the water density is near 50% of the bulk value). This is due to the ability of the nucleophile to keep part of its hydration shell when it is transferred from the aqueous to the organic phase, consistent with experimental observations regarding the "polluting" effect of a few water molecules on the rate of similar reactions.[12−14] The TMA^+ catalyst slightly *increases* the barrier height of this reaction when it is associated with the Cl^- nucleophile,[11] consistent with bulk experimental studies showing reduced reactivity when the anion is ion-paired.[15] Thus, the most effective role of the phase transfer catalyst is to bring the nucleophile a few nanometers into the organic phase, with a minimal number of associated water molecules.

As is clear from our earlier findings and the schematic depiction in Figure 1, the LLPTC process is crucially dependent on (1) the ability of the catalyst to form a relatively stable ion pair with the reactant, (2) a favorable partitioning in the organic phase, and (3) a return to the interface so the process can be repeated. In this paper, we focus on the molecular aspects of the ion and ion-pair transport across the interface, as well as the ion-pair dissociation/recombination process by calculating several equilibrium-free energy functions

Special Issue: Paul F. Barbara Memorial Issue

Received: July 5, 2012
Revised: October 3, 2012
Published: October 17, 2012

   dx.doi.org/10.1021/jp306669t | J. Phys. Chem. B 2013, 117, 4325−4331

and examining nonequilibrium trajectories involving $(C_4H_9)_4N^+Cl^-$ at the water/chloroform interface. The calculations reported below examine the factors that influence the stability and the transport of the ion pair and in particular the correlation with local surface structure, since it is well-known that ions and ion pairs transported across organic/aqueous interfaces may be accompanied by water molecules.[4,16−18] We should mention here that several groups have examined the distributions of ions across the water/chloroform interface. In particular, Wipff and co-workers examine the distribution of ions of different sizes and charges at the interface,[19,20] and Chang and Dang examine ion transfer across the water/chloroform interface.[21] Very recently, Morita and co-workers published molecular dynamics calculations of the free energy profiles for the transfer of $(C_4H_9)_4N^+Cl^-$ as well as the individual ions across the water/chloroform interface.[22]

II. SYSTEMS AND METHODS

The simulation system includes 500 water molecules, 213 $CHCl_3$ molecules, and a variety of solute species (described below) in a box of cross section 100 Å × 25 Å × 25 Å. This geometry gives rise to a single liquid/liquid interface, with each bulk phase at equilibrium with its own vapor. The distance normal to the interface is denoted by Z, and the location of the Gibbs dividing surface (the plane where the average water density is half the bulk value) is at $Z = 0$. On average, the water occupies the $Z < 0$ region and the chloroform the $Z > 0$ region of the simulation box. See Figure 2.

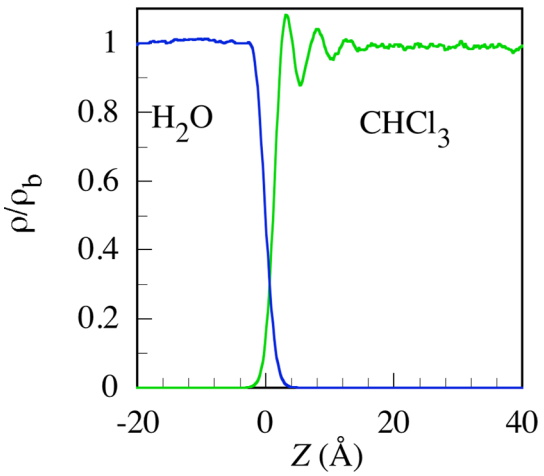

Figure 2. The density profile (298 K) of the water and chloroform liquids in the system under study.

In general, the equilibrium behavior of the X^-Q^+ ion pair at the liquid/liquid interface can be fully characterized by computing the free energy as a function of: (a) the location of the ion-pair center of mass z_{cm} along the interface normal, (b) the X−Q bond distance R, and (c) the orientation of the X−Q vector with respect to the interface normal. The prohibitively long computation of this four-dimensional object is further complicated by the fact that the surface structure, and in particular the water local density, is strongly coupled to the variables listed above. For example, as the ion pair dissociates or as one of the ions crosses into the organic phase, some portion of the ion hydration shell may be dragged along.

To make the quantitative description of the free-energy landscape more manageable, we instead compute several projections of the full free energy function as follows:

(1) The free energy profiles $W(z)$ of the ions Cl^-, $(CH_3)_4N^+$ (TMA^+), and $(C_4H_9)_4N^+$ (TBA^+) across the liquid/liquid interface.
(2) The free energy profile $W(z_{cm})$ of the ion pairs $(CH_3)_4N^+Cl^-$ (TMACl) and $(C_4H_9)_4N^+Cl^-$ (TBACl) across the liquid/liquid interface. The ion-pair bond distance R is constrained to its equilibrium value in bulk chloroform, $R = R_{eq}$.
(3) The ion-pair potential of mean force $W(R)$, while the ion-pair center of mass is at different surface locations and orientations, as well as in the bulk liquids.

Additional insight into the behavior of the ion pair can be obtained by an examination of a nonequilibrium ensemble of trajectories, starting from an ion pair adsorbed at the interface.

The individual ion free energy profiles $W(z)$ and the ion-pair free energy profiles $W(z_{cm})$ are calculated using umbrella sampling with overlapping windows.[23] In each case, 48 windows (2 Å wide with a 1 Å overlap between adjacent windows) are run on a 48-processor Linux cluster (1 ns at each window). The 49 Å total distance is sufficient to map the free-energy profiles from bulk water to bulk chloroform. The ion-pair potentials of mean force $W(R)$ are calculated using umbrella sampling along R, while the ion-pair center of mass is restricted to be in a window whose center Z_w is fixed relative to the Gibbs surface. Seven windows (1 Å wide with a 0.5 Å overlap between adjacent windows) are used. The calculations in bulk chloroform and in the gas phase utilize non-Boltzman sampling using the biasing potential: $U_{bias} = [100\ (kcal/mol)]/[R\ (Å)]$, which greatly improves the statistical accuracy.[24] As will become clear below, no such biasing is required when the ion pair is at the interface or in bulk water.

The calculations in bulk solvents are done in separate truncated octahedron (TO) boxes to avoid possible surface effects. The bulk chloroform box contains 214 chloroform molecules and the ion pair in a TO box enclosed in a cube of size 38.68 $Å^3$. The bulk water box contains 960 molecules and the ion pair in a TO box enclosed in a cube of size 39.11 $Å^3$. (These box sizes are adjusted to give a pressure of 1 atm.)

All equilibrium-free energy calculations are done (using in-house developed molecular dynamics code) at a constant temperature of $T = 298$ K using a combination of the Andersen stochastic method and the Nose−Hoover thermostat.[25] The integration time step is 0.5 fs for all systems, using the velocity version of the Verlet algorithm.[24]

The potential energy functions for the water, chloroform, Cl^-, and TMA^+ were described in our previous publications.[11] For TBA^+, we use a fully flexible united atom model described by Slusher and Cummings,[26] which is based in part on the work of Jorgensen and Gao.[27]

III. RESULTS AND DISCUSSION

1. Free Energy Profiles. The results for the free energy profiles of the ions and ion pairs studied are shown in Figure 3.

Each free energy profile $W(z)$ is shown relative to the value in bulk water. The qualitative behavior of the different species is as expected given their size and total charge. $W(z)$ for the hydrophilic ion Cl^- rapidly increases upon the transfer from water to chloroform. The free energy of transfer being $\Delta A_t = W(\text{bulk } CHCl_3) - W(\text{bulk } H_2O) = 14.5$ kcal/mol. The

dx.doi.org/10.1021/jp306669t | J. Phys. Chem. B 2013, 117, 4325−4331

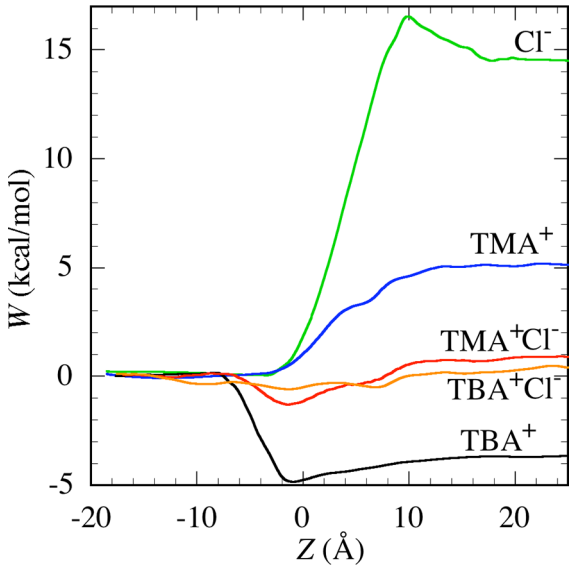

Figure 3. The free energy profiles of different ions and ion pairs (as indicated) across the water/chloroform interface relative to the free energy in bulk water. The water occupies the $Z < 0$ region and the chloroform the $Z > 0$.

corresponding values for the larger TMA^+ and TBA^+ ions are +5 and −3.5 kcal/mol, respectively, corresponding to their increased size and hydrophobicity. These values are consistent with experimentally reported values for the transfer of these ions between water and similar solvents.[28] The binding of Cl^- to each cation gives rise to a neutral species with a slightly positive free energy of transfer (+1 and +0.5 kcal/mol for TMA^+Cl^- and TBA^+Cl^-, respectively). These values underscore the ability of the phase transfer catalyst to transfer the hydrophilic ion across the interface.

The shape of the free energy profile provides additional insight into the nature of the species−solvent interactions. The slight barrier to the back transfer of the Cl^- to the aqueous phase (approximately 2 kcal/mol at z = 10 Å) can be understood as the additional free energy required to create a water finger that extends into the organic phase. This structural motif (that exists to a much smaller extent for the other species) will be demonstrated below. In contrast, the free energy profile of the hydrophobic cation TBA^+ and the ion pairs exhibits shallow minima near the Gibbs surface, reflecting the competition between the driving force to restore the water−water hydrogen bonding and the water−ion electrostatic interaction.

More detailed information about the solute−solvent interaction is provided in Figure 4, which shows the average of the total ion−solvent interaction energies as a function of the distance of the solute center of mass along the interface normal.

This plot suggests interesting differences in the transfer mechanism of the different ions and ion pairs. The more step-like change in the interaction between the Cl^- and the two solvents reflects the ability of the Cl^- to maintain stronger hydration across a longer distance, with the final drop in H_2O−Cl^- energy taking place at the location of the barrier previously identified. This sudden drop occurs at smaller z values when the Cl^- is a member of the ion pair, and it is more abrupt (compared with the single ion) and represents a somewhat larger fraction of the total energy. The normalization of all interaction energies by the ion−solvent bulk values helps

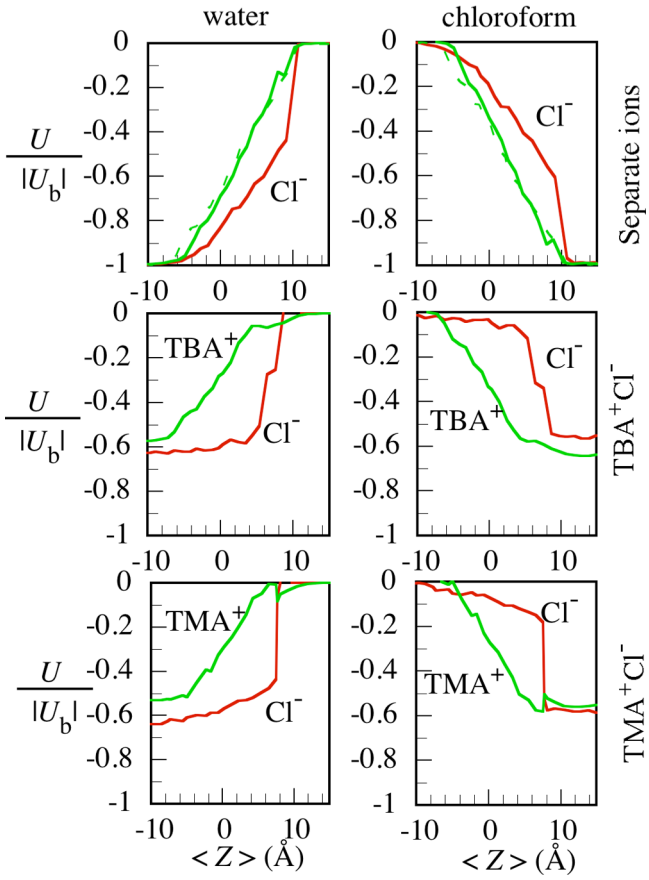

Figure 4. Average ion−water (left panels) and ion−chloroform (right panels) interaction energies vs the location along the interface normal of the solute's center of mass. The top two panels are for the individual ions (the solid and dashed unlabeled green lines are for TMA^+ and TBA^+, respectively). In the middle and bottom panels, the ions are combined as ion pairs as indicated. The energies are normalized by the total interaction energy of the individual ions in the bulk solvents. (U_b = −154, −110, and −116 kcal/mol for the interaction between water and Cl^-, TMA^+, and TBA^+, respectively; U_b = −88, −65, and −75 kcal/mol for the corresponding interactions with chloroform.)

demonstrate the remarkable near conservation of the total ion solvation energy upon transfer:

$$\frac{U_{I-W}(z)}{|U_{I-W}^{bulk}|} + \frac{U_{I-C}(z)}{|U_{I-C}^{bulk}|} \approx \begin{cases} -1.0 \pm 0.02 & \text{for any bare ion I} \\ -0.6 \pm 0.04 & \text{for any ion I belonging to an ion pair} \end{cases} \quad (1)$$

where $U_{I-W}(z)$ and $U_{I-C}(z)$ are the average ion−water and ion−chloroform interaction energies at location z, respectively. For example, when TBA^+ is transferred from water to chloroform, any percent reduction in its interaction with water is replaced by the same percent increase interaction with chloroform. The same applies when TBA^+ is part of the TBA^+Cl^- ion pair, except that, in this case, this interaction is only 60% of the interaction of the bare ion. This is due to the fact that not all the water (or the chloroform) molecules interacting with the ion pair are optimally oriented to interact with each individual ion compared to the case where the ions are unpaired.

dx.doi.org/10.1021/jp306669t | J. Phys. Chem. B 2013, 117, 4325−4331

The continuous replacement of water by chloroform molecules (gradual or abrupt) can also be demonstrated by considering the structure of the ions' first solvation shell. This is depicted in Figure 5, which shows the peak value of the ion−

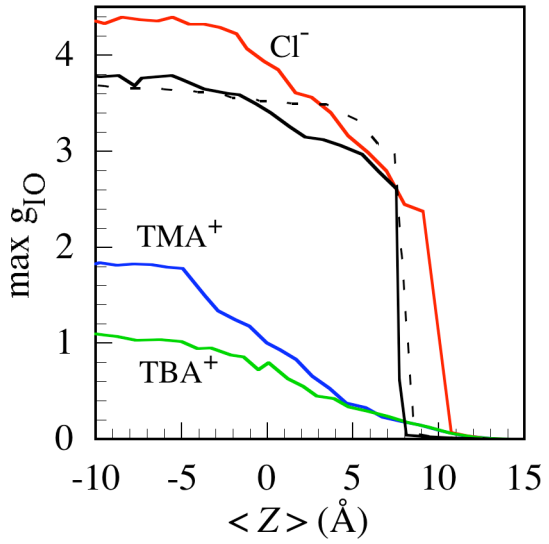

Figure 5. Peak value of the oxygen (water)−ion radial distribution function vs ion location along the interface normal. The labeled lines correspond to the bare ions, and the unlabeled solid and dashed lines correspond to water−chloride max{$g(r)$} in TMA^+Cl^- and TBA^+Cl^-, respectively.

oxygen orientationally averaged radial distribution function calculated from configurations where the ion samples all locations within a slab parallel to the interface, vs the slab location.

The abrupt drop in the water−bare Cl^- $g(r)$ peak value at z = 10 Å and, to a slightly greater degree (at smaller values of z), when the Cl^- is paired with the cation (unlabeled solid and dashed lines) mirrors the behavior of the interaction energy shown in Figure 4.

The observed variations of the water−ion interaction energy and the peak value of the water−ion radial distribution functions can be quantitatively correlated with specific structural changes of the interface as follows: at any given configuration, we identify all the water molecules that are members of a continuous structure connected with bulk water molecules. Any water molecule that belongs to this structure must have at least one hydrogen bond to another molecule already identified as belonging to this structure. Let h_W be the center of mass location of the water molecule (a member of this structure) with the largest value of z. When the solute is located in a slab whose center is at Z, the observed values of h_W can be characterized by a distribution $P(h_W; Z)$ or simply by the average $\langle h_W(Z)\rangle$. Figure 6 shows this average vs Z for the different solutes studied.

When the solute's center of mass is located outside the interface region ($Z < -5$ Å or $Z > 15$ Å), the average maximum water protrusion relative to the Gibbs surface is near h_W = 2 Å and is independent of the solute's location. It simply reflects the size of the neat interface. This protrusion becomes significantly larger when the solutes' enter the interface region. The magnitude of the protrusion and its dependence on the solute's location is very sensitive to the nature of the solute. As soon as Cl^- crosses the Gibbs surface, water protrusions appear. These

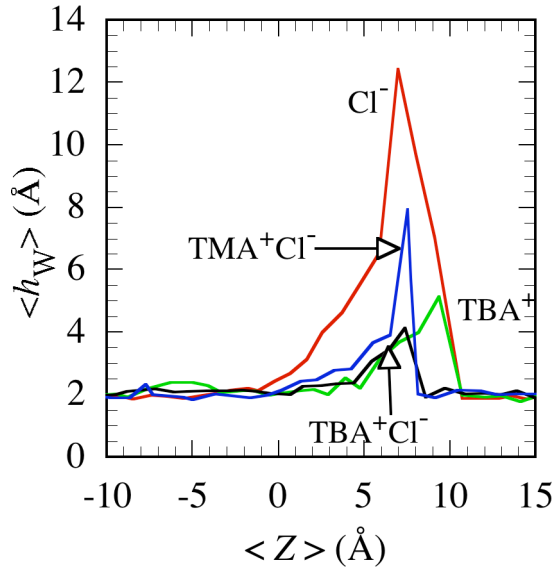

Figure 6. Average maximum protrusion of water into the organic phase vs the solute location.

initially extend about 1 Å beyond the location of the anion, but when the anion is at Z = 7 Å, they reach h_w = 12 Å in size, reflecting the ability of this anion to carry a significant portion of its hydration shell. Once the anion position reaches Z = 11 Å, most of these water molecules are no longer part of a continuous structure reaching back to the bulk water. This corresponds to the drop in values of $g(r)$ and the interaction energy. This behavior is in significant contrast with that of the TBA^+ cation. In this case, water protrusions lag (on average) behind the location of the cation (they reach an average value of h_w = 5 Å when the ion is at Z = 10 Å), although their value is greater than the normal h_w = 2 Å, as long as the cation is in the region Z < 11 Å (like the Cl^-). This behavior correlates with the significantly less dramatic change in the peak value of $g(r)$. Interestingly, the ion pairs are able to create larger protrusions (at smaller Z values than the cations), and returning to the normal value of 2 Å at smaller Z values. This is consistent with these protrusions being mainly connected with the Cl^-. The ion pair is oriented with the Cl^- pointing toward the water phase, so the Cl^- location is a few Å closer to the Gibbs surface than the solute center of mass location. This is reflected by the observed variation in the peak value of $g(r)$, dropping to zero at earlier Z values than that of the bare Cl^-.

We now turn to an examination of the stability of the ion pairs at the interface. The ability of the phase transfer catalyst to carry the anion to the organic phase depends on rapid recombination at the interface followed by relative ease of transfer to the organic phase as a relatively stable species. Thus, it is important to characterize the free energies of the dissociation/recombination reactions $TBA^+Cl^- \leftrightarrow TBA^+ + Cl^-$ and $TMA^+Cl^- \leftrightarrow TMA^+ + Cl^-$ at different interface locations. Figure 7 shows these free energy profiles (or potential of mean force, PMF) vs the interionic distance R at different locations. Note that not included is the effective rotational term $(-2kT \ln R)$, which accounts for the proper volume of phase space when the three-dimensional configuration of the ion pair is projected onto one dimension.[29]

The cation−anion electrostatic attraction gives rise to significant binding energy and to the expected shapes of the PMF in a vacuum. Note that the equilibrium value of R in a

dx.doi.org/10.1021/jp306669t | J. Phys. Chem. B 2013, 117, 4325−4331

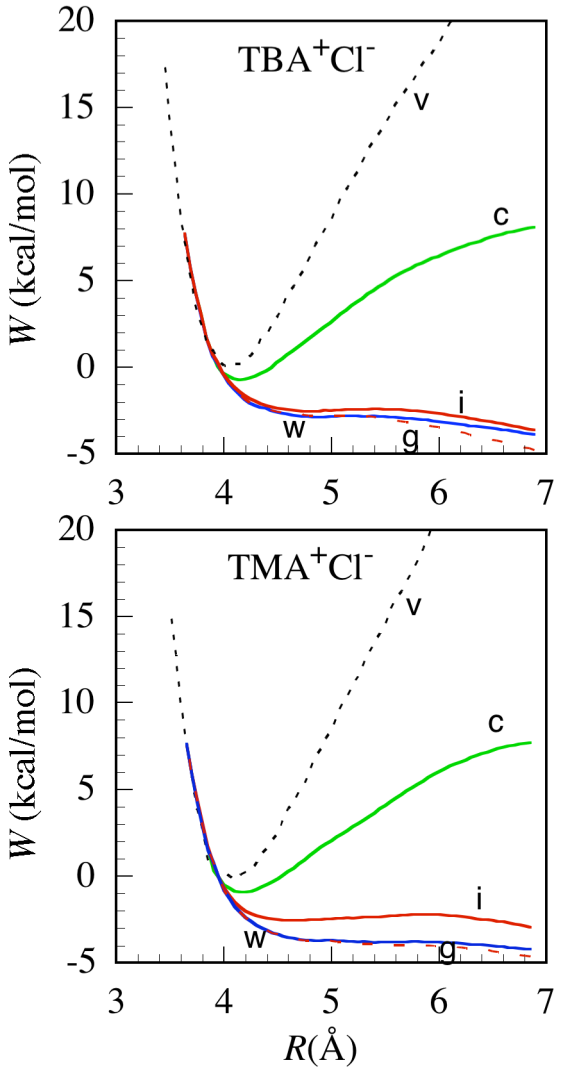

Figure 7. The potential of mean force (PMF) for the dissociation of the TBA^+Cl^- (top panel) and TMA^+Cl^- (bottom panel) ion pairs at different locations of the water/chloroform interface. In each panel, the PMF is shown in a vacuum (dotted line labeled "v"), in bulk water (solid line labeled "w"), in bulk chloroform (solid line labeled "c"), at the Gibbs surface (dashed line labeled "g"), and at a location that is 5 Å into the organic phase relative to the Gibbs surface (solid line labeled "i").

vacuum for the two ion pairs is almost the same despite the different sizes of the two cations,[26] reflecting the ability of the Cl^- to approach the positively charged nitrogen along a line bisecting the CNC angle. While the weakly polar chloroform is able to slightly lower the energy of the separate ions, the ion pair remains quite stable in bulk chloroform but at an equilibrium interionic distance that is slightly larger than in a vacuum. In bulk water, a well-known result is obtained: the significantly more negative hydration free energy of the separate ions (than the contact ions) overcomes the electrostatic attraction and gives rise to a PMF that indicates spontaneous dissociation of both ion pairs to the more stable separate ions.

The PMF at the interface is quite similar to the one in bulk water for both ion pairs. The one calculated when the center of mass of the ion pair is in the slab centered at the Gibbs surface is virtually identical to the one in bulk water, and the one calculated when the center of mass is located at a slab centered 5 Å into the chloroform is only 1.5 kcal/mol higher and shows a slight barrier to dissociation. The facile dissociation at the interface is due to the efficient hydration of the Cl^- by interfacial water molecules. Moving the ion pair toward the organic phase does not diminish the ability of water to provide this hydration, as long as the Cl^- is able to interact with water surface fluctuations ($Z < 10$ Å). This means that, as R increases at large Z, the ion pair reorients so the Cl^- points toward the aqueous phase.

This can be demonstrated by computing the potential of mean force for parallel vs perpendicular orientations, as shown in Figure 8.

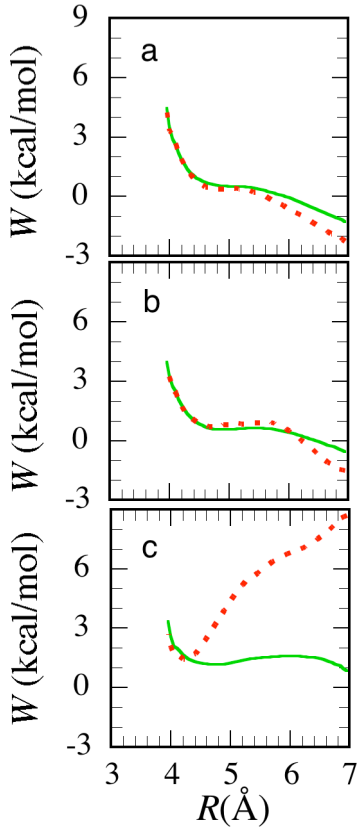

Figure 8. Orientational dependence of the TBA^+Cl^- potential of mean force. The ion-pair center of mass is located at the Gibbs surface (panel a) or 5 Å into the organic phase relative to the Gibbs surface (panels b and c). In panel c, the interface is forced to remain flat (capillary waves are suppressed). In each panel, the solid and dotted lines correspond to the ion-pair interionic vector being perpendicular (with the Cl^- pointing toward the aqueous phase) and parallel to the surface, respectively.

If the ion-pair center of mass is located in a slab that is centered at the Gibbs surface (panel a) or in a slab that is 5 Å away from the Gibbs surface into the organic phase, there is virtually no difference between the PMF calculated at the two different orientations, since the water molecules are able to "find their way" to interacting with the chloride ion. However, if the interface capillaries are suppressed (panel c), only when the chloride ion is in direct contact with the water (which is possible only at the perpendicular orientation) do we have spontaneous dissociation of the ion pair. The PMF for the parallel orientation is quite similar to that in bulk chloroform.

dx.doi.org/10.1021/jp306669t | J. Phys. Chem. B 2013, 117, 4325−4331

These calculations demonstrate the strong coupling between surface capillary fluctuations and the ion-pair bond distance R.

The symmetry-breaking at the interface involved in the different ways the two ions interact with the water can be clearly demonstrated by computing the average normalized ion−solvent interaction energy as a function of the ion-pair bond distance, as shown in Figure 9.

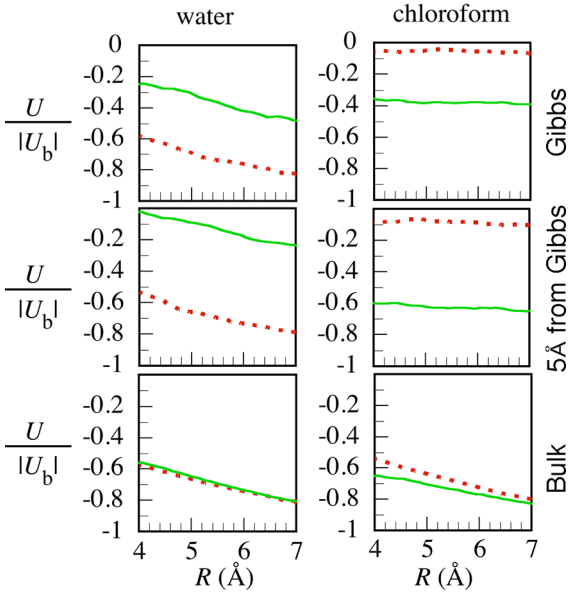

Figure 9. Average normalized ion−water (left panels) and ion−chloroform (right panels) interaction energies as a function of the TBA^+Cl^- interionic distance. The panels from top to bottom are for the ion pair located at the Gibbs surface, 5 Å into the organic phase and in the bulk solvent. The energies are normalized by the interaction energy of the individual ions in the bulk solvents (U_b). In each panel, the green solid line is for TBA^+ and the red dotted line for Cl^-.

As the ion pair dissociates, the buildup of the full hydration shell around the separate ions is clearly demonstrated by the negative slope lines in the left panels. However, while the lines for the cations and anions fall on top of each other in the bottom panel (reflecting the symmetrical bulk environment), the clear separation in the two top panels (and more so when the ion is on the organic side of the Gibbs surface) is consistent with the ability of the chloride to favorably interact with the water to a degree that is quite similar to that in the bulk (the red dotted lines in the three panels are almost identical to each other). A parallel picture emerges when the interactions of the two ions with chloroform are shown in the right panels.

Finally, we briefly discuss the nonequilibrium dynamics of the ion-pair dissociation and transport. We consider the question to what degree the free-energy profiles described above provide a qualitative explanation of the dynamics. Starting from an initial distribution of TBA^+Cl^- ion pairs whose center of mass is located approximately 5 Å from the Gibbs surface in the organic phase, we follow the dynamics of 100 independent trajectories for 60 ps each. The results are shown in Figure 10.

An examination of the TBA^+Cl^- bond distance distribution $P(R; t)$ (not shown) shows rapid dissociation consistent with the barrier-less PMF along R (Figure 7). Figure 10 shows that this rapid dissociation involves the transfer of the Cl^- into the aqueous phase and the simultaneous adsorption of TBA^+ at the

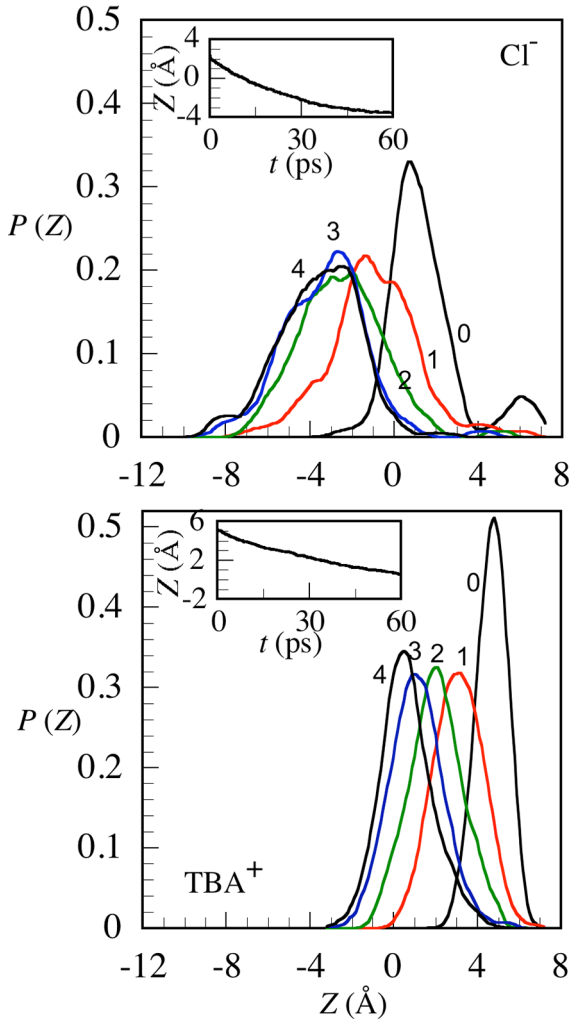

Figure 10. Probability distributions $P(Z; t)$ of the location of TBA^+ (bottom panel) and Cl^- (top panel) ions vs time. Each curve is obtained by binning the positions from 100 trajectories using a 3 ps window. In each panel, curves 0, 1, ..., 4 correspond to $0 < t < 3$ ps, 12 ps $< t <$ 15 ps, ..., 57 ps $< t <$ 60 ps. The insets show the average position vs time.

interface, both consistent with the free energy profiles shown in Figure 3. Note that, while the probability distribution of the chloride ion location shows significant broadening as the ion diffuses into the aqueous phase, the distribution for the cation shifts toward the Gibbs surface with only minor spreading. A small fraction of the initial ion pairs were oriented with the anion pointing toward the organic phase (reflected in the small second peak of the initial probability distribution). These ion pairs experience a slight delay in dissociation, but as they diffuse and reorient, they also experience rapid dissociation. It is also worthwhile noting that, as expected, the interaction of the two ions with the water shows increased hydration, while there is a slight desolvation with respect to chloroform.

IV. SUMMARY AND CONCLUSIONS

Molecular dynamics calculations of the free energy functions relevant to the fundamental processes associated with the operation of phase transfer catalysts (PTC) have been presented. The interfacial recombination of the alkyl ammonium PTC with a simple nucleophile to produce an ion pair facilitates the transport to the organic phase. Rapid

dx.doi.org/10.1021/jp306669t | J. Phys. Chem. B 2013, 117, 4325−4331

dissociation and recombination at the interface are due to significant interfacial hydration made possible by water density fluctuations. A detailed examination of solvent−solute interaction energies and water structure provides molecular-level insight consistent with the equilibrium free energy functions. The dynamics of the ion-pair dissociation and transport are also consistent with these free energy functions.

The set of PMF functions calculated suggests the following mechanism for the facilitated transfer of a chloride ion from water to chloroform: Starting from a free Cl^- on the water side of the interface, a rapid binding with the catalyst at the interface will generally produce an unstable ion pair, which may immediately dissociate (Figure 8a and b). However, a fluctuation that orients the Cl^- toward the organic phase or a fluctuation that reduces the size of a water finger can create a metastable ion-pair (Figure 8c), which can diffuse to the chloroform phase where it is quite stable (Figure 7). Figure 3 shows that TBA^+'s advantage over TMA^+ is in providing a higher concentration of Cl^- in chloroform. This mechanism is consistent with recent experiments showing that the activity of a set of tetraalkylammonium phase transfer catalysts is correlated with their concentration in the organic phase.[30]

AUTHOR INFORMATION

Notes

The authors declare no competing financial interest.

ACKNOWLEDGMENTS

This work has been supported by a grant from the National Science Foundation (CHE-0809164).

REFERENCES

(1) Starks, C. M.; Liotta, C. L.; Halpern, M. *Phase Transfer Catalysis*; Chapman & Hall: New York, 1994.
(2) Makosza, M. *Pure Appl. Chem.* **2000**, *72*, 1399−1403.
(3) Albanese, D. *Catal. Rev.: Sci. Eng.* **2003**, *45*, 369−395.
(4) *Interfacial Catalysis*; Volkov, A. G., Ed.; Marcel Dekker: New York, 2003.
(5) Eckert, C. A.; Liotta, C. L.; Bush, D.; Brown, J. S.; Hallett, J. P. *J. Phys. Chem. B* **2004**, *108*, 18108−18118.
(6) Albanese, D. *Mini-Rev. Org. Chem.* **2006**, *3*, 195−217.
(7) Shao, Y. H.; Mirkin, M. V.; Rusling, J. F. *J. Phys. Chem. B* **1997**, *101*, 3202−3208.
(8) Benjamin, I. *J. Chem. Phys.* **2008**, *129* (074508), 1−11.
(9) Nelson, K. V.; Benjamin, I. *J. Chem. Phys.* **2009**, *130* (194502), 1−9.
(10) Nelson, K. V.; Benjamin, I. *J. Phys. Chem. C* **2010**, *114*, 1154−1163.
(11) Nelson, K. V.; Benjamin, I. *J. Phys. Chem. C* **2011**, *115*, 2290−2296.
(12) Landini, D.; Maia, A.; Rampoldi, A. *J. Org. Chem.* **1989**, *54*, 328−332.
(13) Maia, A. *Pure Appl. Chem.* **1995**, *67*, 697−702.
(14) Albanese, D.; Landini, D.; Maia, A.; Penso, M. *Ind. Eng. Chem. Res.* **2001**, *40*, 2396−2401.
(15) Reichardt, C. *Solvents and Solvent Effects in Organic Chemistry*, 2nd ed.; Springer-Verlag: Weinheim, Germany, 1988.
(16) Benjamin, I. *J. Phys. Chem. B* **2008**, *112*, 15801−15806.
(17) Rose, D.; Benjamin, I. *J. Phys. Chem. B* **2009**, *113*, 9296−9303.
(18) Bisson, P.; Xiao, H.; Kuo, M.; Kamelamela, N.; Shultz, M. J. *J. Phys. Chem. A* **2010**, *114*, 4051−4057.
(19) Berny, F.; Schurhammer, R.; Wipff, G. *Inorg. Chim. Acta* **2000**, *300*, 384−394.
(20) Schurhammer, R.; Wipff, G. *J. Mol. Struct.: THEOCHEM* **2000**, *500*, 139−155.
(21) Chang, T. M.; Dang, L. X. *J. Phys. Chem. B* **1997**, *101*, 10518−10526.
(22) Kikkawa, N.; Ishiyama, T.; Morita, A. *Chem. Phys. Lett.* **2012**, *534*, 19−22.
(23) Chandler, D. *Introduction to Modern Statistical Mechanics*; Oxford University Press: Oxford, U.K., 1987.
(24) Allen, M. P.; Tildesley, D. J. *Computer Simulation of Liquids*; Clarendon: Oxford, U.K., 1987.
(25) Nosé, S. *J. Phys.: Condens. Matter* **1991**, *2*, SA115−SA119.
(26) Slusher, J. T.; Cummings, P. T. *J. Phys. Chem. B* **1997**, *101*, 3818−3826.
(27) Jorgensen, W. L.; Gao, J. *J. Phys. Chem.* **1986**, *90*, 2174−2182.
(28) Marcus, Y. *Ion Solvation*; Wiley: New York, 1985.
(29) Rodger, P. M.; Sceats, M. G. *J. Chem. Phys.* **1985**, *83*, 3358−3362.
(30) Denmark, S. E.; Weintraub, R. C.; Gould, N. D. *J. Am. Chem. Soc.* **2012**, *134*, 13415−13429.